Electronic Supplementary Material (ESI) for ChemComm.

Supporting information for

Influence of transition metal electronegativity on the oxygen storage capacity of perovskite oxides

Lu Liu, [a] Daniel D. Taylor, [b] Efrain E. Rodriguez[a] and Michael R. Zachariah*[a,c]

a. Department of Chemistry and Biochemistry, University of Maryland, College Park, MD 20742, USA

b. Department of Material Science and Engineering, University of Maryland, College Park, MD 20742, USA

c. Department of Chemical and Biomolecule Engineering, University of Maryland, College Park, MD 20742, USA

S1. Experimental methods

Materials. All perovskites were synthesized in our laboratory using aerosol-assisted spray pyrolysis with metal nitrate aqueous solutions as precursors. All chemicals were obtained from Sigma-Aldrich, including $La(NO_3)_3·6H_2O$ (≥99.0% pure), $Ca(NO_3)_3·4H_2O$ (≥99.0% pure), $Mn(NO_3)_2·4H_2O$ (≥97.0% pure), $Fe(NO_3)_3·9H_2O$ (≥98% pure), $Ni(NO_3)_2·6H_2O$ (≥97.0% pure), $Co(NO_3)_2·6H_2O$ (≥98% pure), $Cu(NO_3)_2·3H_2O$ (≥98% pure), $Cr(NO_3)_3·9H_2O$ (≥98% pure), $Ba(NO_3)_2·9H_2O$ (≥98% pure) and $Sr(NO_3)_2·9H_2O$ (≥99% pure). The spray pyrolysis system consists of a stainless steel atomizer, silica-gel diffusion dryer, an isothermal tube furnace, and a stainless steel sample collector, as described in details in previous publications.[1] The synthetic process can be described as a droplet-to-particle method, where the precursor droplets are decomposed into perovskite mixed metal oxides in the isothermal furnace. For the precursor solution, 0.20 M metal nitrates, 0.10 M citrate acid are dissolved in DI water. The atomizer is a collision-type nebulizer, which generates droplets with diameters approximately 1 μm in size. The precursor droplets were carried by compressed air gas with a flow rate of ~3 L/min into the diffusion dryer, then into the isothermal tube furnace at 1050 ^{o}C to decompose the precursors into oxide particles with a ~1s residence time. Finally, particles exiting the aerosol reactor are collected on a 0.4 μm DTTP Millipore filter with 10%-20% porosity (purchased from EMD Millipore).

Material Characterizations. Crystal structures of OCs are characterized by X-Ray Diffraction (XRD) with a Bruker Smart1000 detector using Cu Kα radiation. Transmission Electron Microscopy (TEM) and High Resolution Transmission Electron Microscopy (HRTEM) is performed using a Field Emission Transmission Electron Microscope (JEOL 2100 FE-TEM). Scanning Electron Microscopy (SEM) results are obtained by Hitachi SU-70 SEM. TGA (Thermal Gravimetric Analyzer) coupled MS (Mass spectroscopy) tests were conducted simultaneously in a SDT Q600 coupled with Discovery TM quadruple mass spectrometer from TA instruments, with an alumna sample crucible loaded with ~10 mg samples. Samples were first heated to 150 ^{o}C to and held for 30 min then ramped at 10 ^{o}C min^{-1} to 750 ^{o}C and held for 30 min.

CLC Reactivity test. Total methane oxidation and stability tests of the perovskites were performed in a vertically oriented fixed bed reactor placed in an electrically heated isothermal furnace at 750 ^{o}C. The effluent was sampled with a mass spectrometer (Stanford Research UGA 300) with a mass resolution of <0.5 atomic mass units (amu) at 10% of peak height and a detection limit <1 ppm. Argon was also used as an internal mass spectrometer standard for quantitative analysis of the effluent gases, and Ar flow rate were kept at a fixed value. By varying the flow rates of CH_4 and O_2 with a fixed Ar flow rate, calibrations of the mass spectrometer for different gases with different concentrations, including CO_2, CO, CH_4, H_2.

Nominally, a ~200 mg oxygen carrier sample is used for each test. The quartz flow reactor has a length of 61 cm, with a 1 cm inner diameter. The particles are first annealed at the reaction temperature for 1 hour, and then exposed alternatively to 11% methane for 2 min and 20% oxygen for 5 min simulating the CLC reactor. Argon is introduced for 300 s after each period, to purge the reactor and avoid oxygen and methane mixing between the oxidation and reduction cycles. We achieved 50 cycles in this test and more details can be found in our previous study.[2]

S2. Results

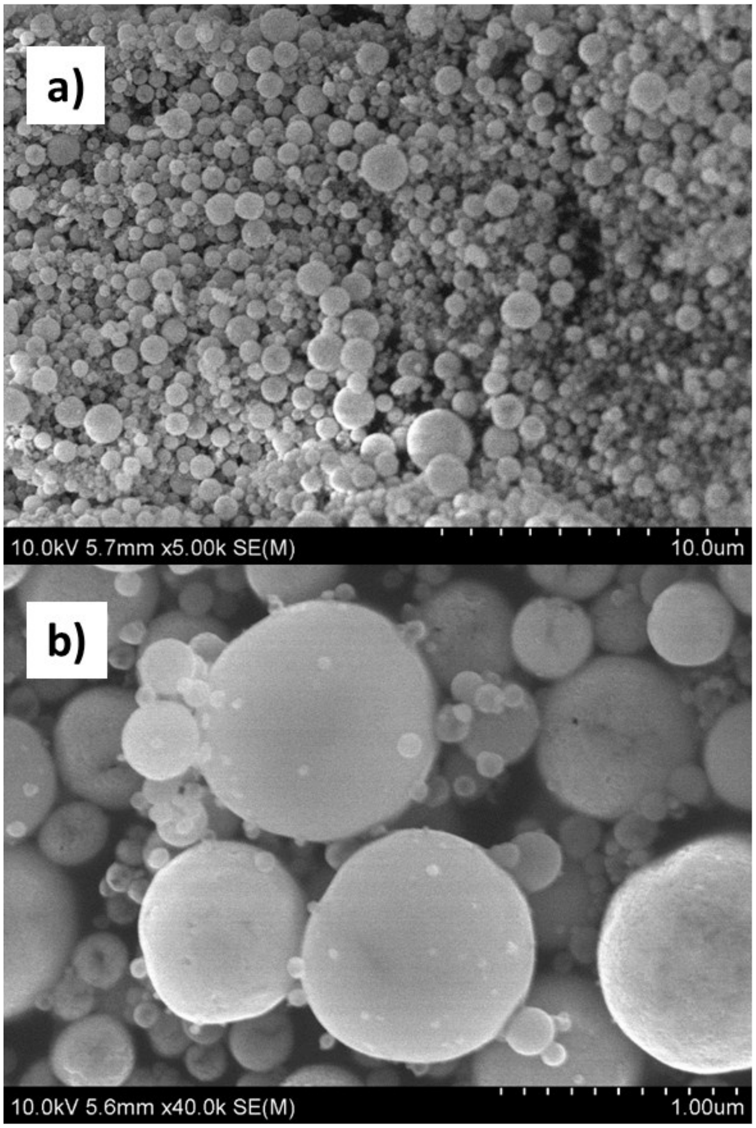

Figure S1. SEM of $LaCrO_3$ 1a) and 1b) shows the spherical morphology and 1c) XRD images indicates the perovskite crystal structures (solid stars) of as-synthesized perovskites (diamonds indicates trace amount of $La_{0.87}Mn_{0.88}O_{3.29}$ (JCPDS card No. 01-077-9446))

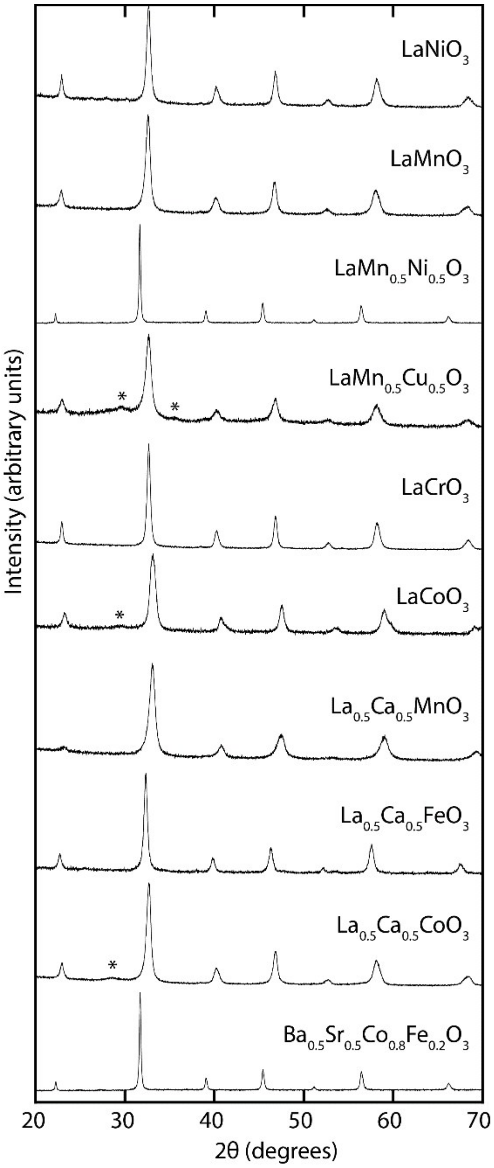

Figure S2. Powder XRD patterns for each of the tested samples. All samples were pseudocubic perovskites with Le Bail refinement performed in either the cubic (*Pm*-3*m*), orthorhombic (*Pbnm*), or rhombohedral (*R*-3*c*) space groups. Select refinement parameters are provided in Table S1. Asterisks indicate the locations of small, broad possible impurity peaks. $LaCoO_3$ and $La_{0.5}Ca_{0.5}CoO_3$ both had a weak peak at approximately 28.5° 2θ. This corresponds to a d-spacing of approximately 3.0 Å. This peak could be attributed to La_2O_3; however, it is not possible to definitively identify this phase as there are no other impurity peaks present in the patterns. For $LaMn_{0.5}Cu_{0.5}O_3$ there are impurity peaks present at approximately 29.5° and 35.5° 2θ. These correspond to d-spacings of 3.0 and 2.5 Å, respectively. The peak at 29.5° 2θ can possibly be attributed to La_2O_3 or Cu_2O, and the peak at 35.5° to CuO. As with the previous samples, the lack of additional impurity peaks makes the definitive identification of these phases impossible. This impurity is poorly crystalline as evidenced by the very broad peak in the low angle data. Other phases considered but ruled out include calcium oxide and carbonate, binary metal oxides, the metallic elements, and all oxygen deficient perovskite based phases present in the ICDD PDF-2 database.

Table S1. Le Bail refinement results for as synthesized samples

			lattice parameters			
	Phase Symmetry	**Crystallite size (nm)**[a]	**a (Å)**	**b (Å)**	**c (Å)**	**volume (Å^3)**
$LaNiO_3$	rhombohedral (*R*-3*c*)	25.4(2)	5.5058(4)		13.372(1)	351.13(6)
$LaMnO_3$	rhombohedral (*R*-3*c*)	20.1(1)	5.5190(4)		13.396(1)	353.37(7)
$LaMn_{0.5}Ni_{0.5}O_3$	rhombohedral (*R*-3*c*)	77.8(5)	5.6407(2)		13.8478(5)	381.80(3)
$LaMn_{0.5}Cu_{0.5}O_3$	cubic (*Pm*-3*m*)	13.1(1)	3.8888(7)			58.81(3)
$LaCrO_3$	orthorhombic (*Pbnm*)	34.3(2)	5.4695(3)	5.5177(3)	7.7598(5)	234.13(2)
$LaCoO_3$	rhombohedral (*R*-3*c*)	20.4(1)	5.4365(5)		13.130(2)	336.08(8)
$La_{0.5}Ca_{0.5}MnO_3$	cubic (*Pm*-3*m*)	12.7(1)	3.8376(4)			56.52(2)
$La_{0.5}Ca_{0.5}FeO_3$	orthorhombic (*Pbnm*)	25.6(2)	5.537(1)	5.571(1)	7.8556(5)	242.30(7)
$La_{0.5}Ca_{0.5}CoO_3$	rhombohedral (*R*-3*c*)	21.5(1)	5.4816(4)		13.535(1)	352.21(6)
$Ba_{0.5}Sr_{0.5}Co_{0.8}Fe_{0.2}O_3$	cubic (*Pm*-3*m*)	66.3(4)	3.9927(1)			63.652(5)

[a] determined from the Scherrer equation

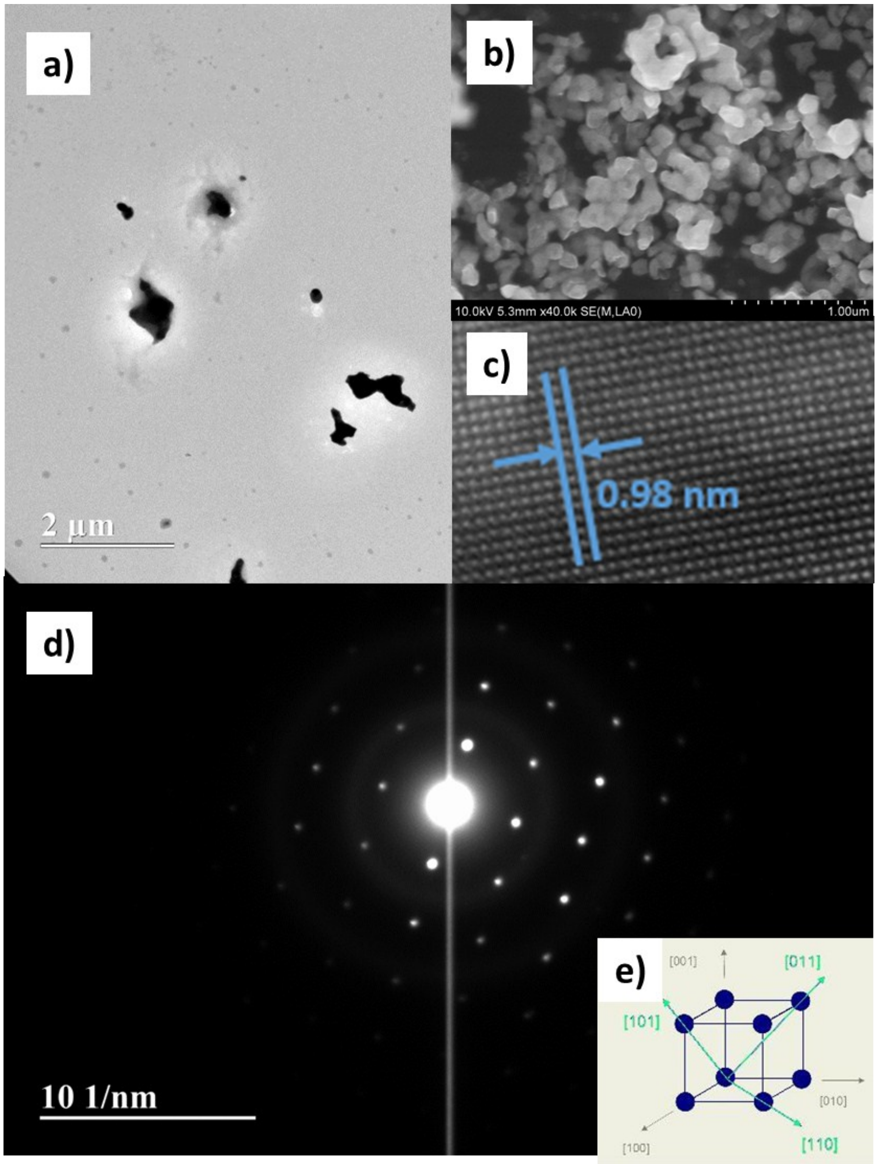

Figure S3. a) TEM, b) SEM and c) HRTEM and d) SAED shows the perovskite crystal structure of the post-reaction $La_{0.5}Ca_{0.5}CoO_3$

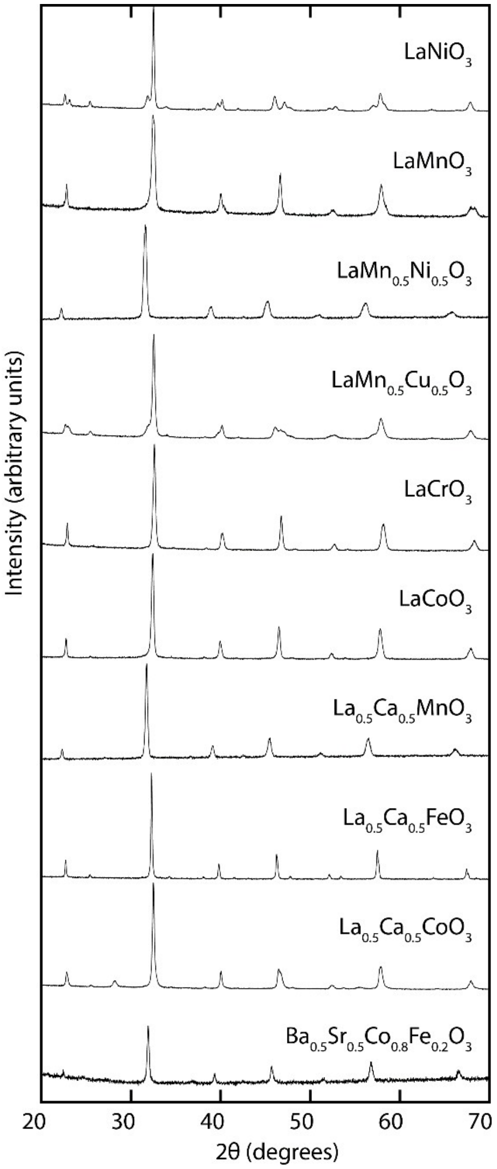

Figure S4. Powder XRD of post fixed bed reactor study samples. All peaks were indexed in either the cubic (*Pm*-3*m*), orthorhombic (*Pbnm*), or rhombohedral (*R*-3*c*) space groups. Select refinement parameters from Le Bail fitting are provided in Table S2.

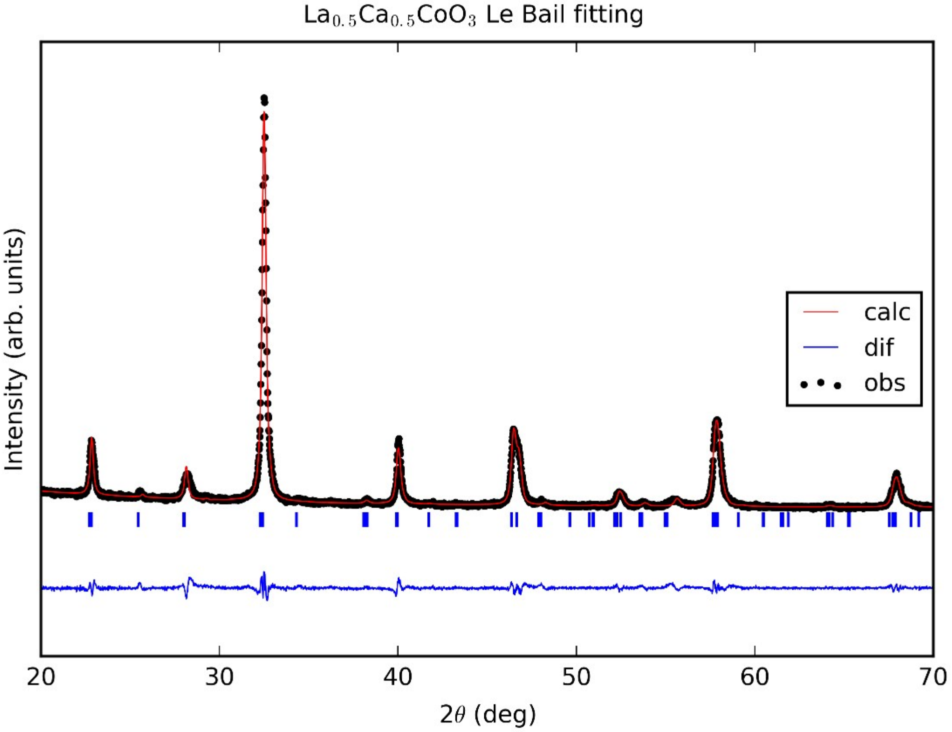

Figure S5. Le Bail fitting of $La_{0.5}Ca_{0.5}CoO_3$ in the orthorhombic *Pnma* space group. Shown are the observed (black circles), refined (red line), difference (blue line) and locations of allowed reflections (blue tick marks).

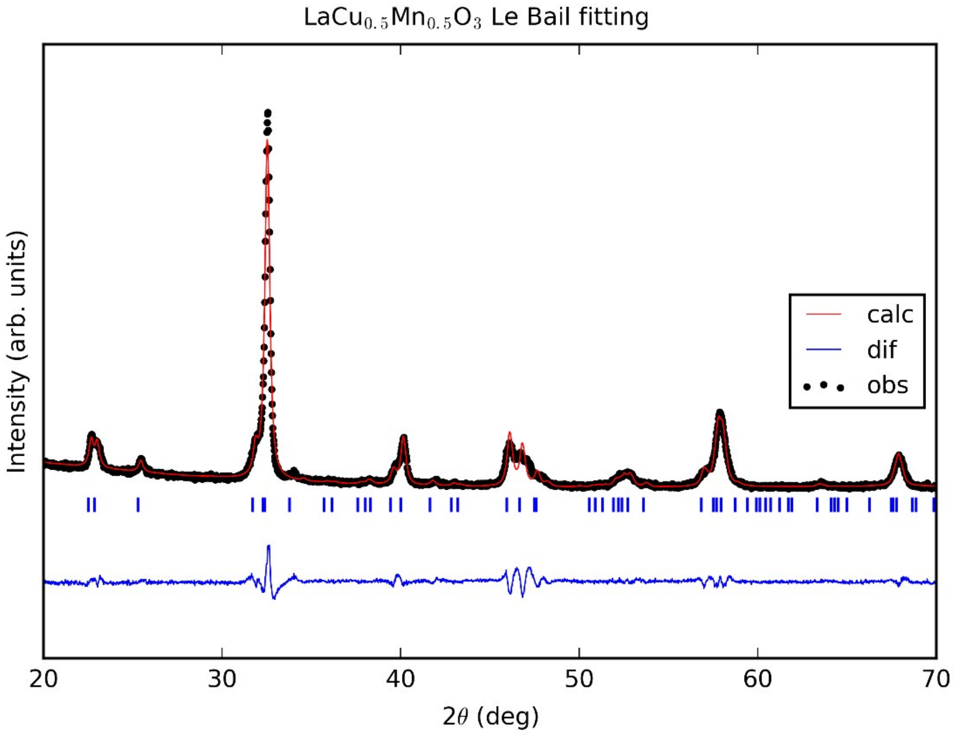

Figure S6. Le Bail fitting of LaCu$_{0.5}$Mn$_{0.5}$O$_3$ in the orthorhombic *Pbnm* space group. Shown are the observed (black circles), refined (red line), difference (blue line) and locations of allowed reflections (blue tick marks).

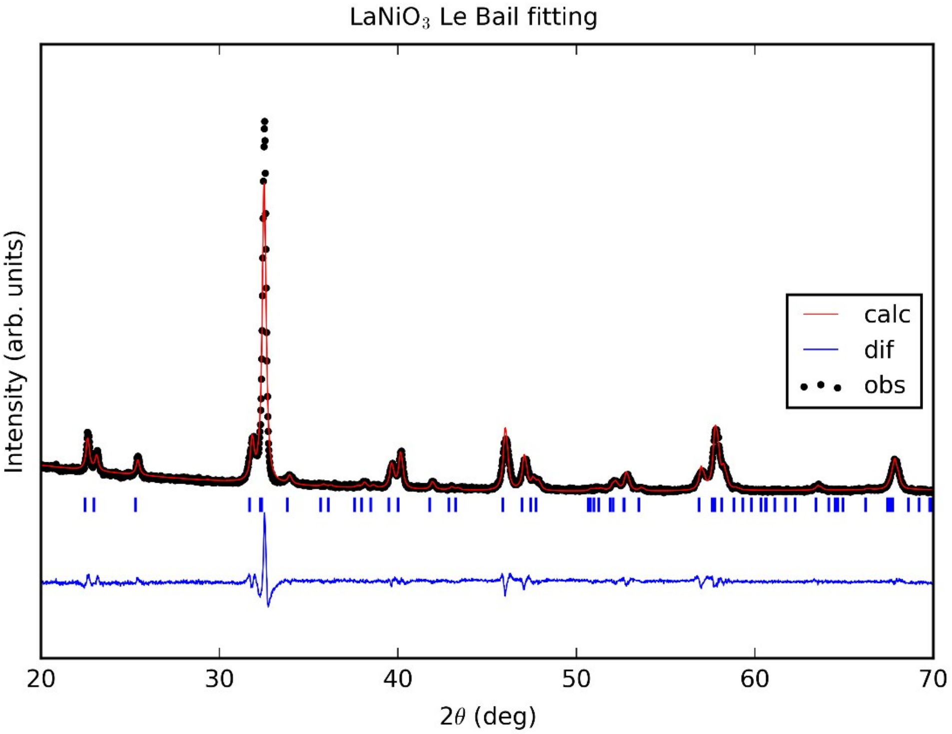

Figure S7. Le Bail fitting of LaNiO$_3$ in the orthorhombic *Pbnm* space group. Shown are the observed (black circles), refined (red line), difference (blue line) and locations of allowed reflections (blue tick marks).

Table S2. Le Bail refinement results for samples post fixed bed reactor studies

			lattice parameters			
	Phase Symmetry	**Crystallite size (nm)**[a]	**a (Å)**	**b (Å)**	**c (Å)**	**volume (Å^3)**
$LaNiO_3$	orthorhombic (*Pbnm*)	57.8(5)	5.5394(4)	5.6513(3)	7.7449(4)	242.45(3)
$LaMnO_3$	rhombohedral (*R*-3*c*)	38.8(4)	5.5193(3)		13.402(1)	353.56(5)
$LaMn_{0.5}Ni_{0.5}O_3$	rhombohedral (*R*-3*c*)	48.1(5)	5.7053(5)		13.870(1)	390.96(7)
$LaMn_{0.5}Cu_{0.5}O_3$	orthorhombic (*Pbnm*)	38.1(3)	5.5260(4)	5.6385(5)	7.7792(6)	242.39(3)
$LaCrO_3$	orthorhombic (*Pbnm*)	67.3(5)	5.5149(2)	5.4776(2)	7.7610(4)	234.45(2)
$LaCoO_3$	orthorhombic (*Pbnm*)	63.6(5)	5.5072(3)	5.5361(2)	7.7941(4)	237.62(2)
$La_{0.5}Ca_{0.5}MnO_3$	orthorhombic (*Pbnm*)	70.6(8)	5.6727(3)	5.6513(4)	7.9691(5)	255.47(3)
$La_{0.5}Ca_{0.5}FeO_3$	orthorhombic (*Pbnm*)	136(1)	5.5646(2)	5.5539(2)	7.8519(2)	242.67(1)
$La_{0.5}Ca_{0.5}CoO_3$	orthorhombic (*Pnma*)	58(1)	5.5384(7)	5.5467(5)	7.7779(5)	238.94(4)
$Ba_{0.5}Sr_{0.5}Co_{0.8}Fe_{0.2}O_3$	cubic (*Pm*-3*m*)	53.7(8)	3.9763(3)			62.87(2)

[a] determined from the Scherrer equation

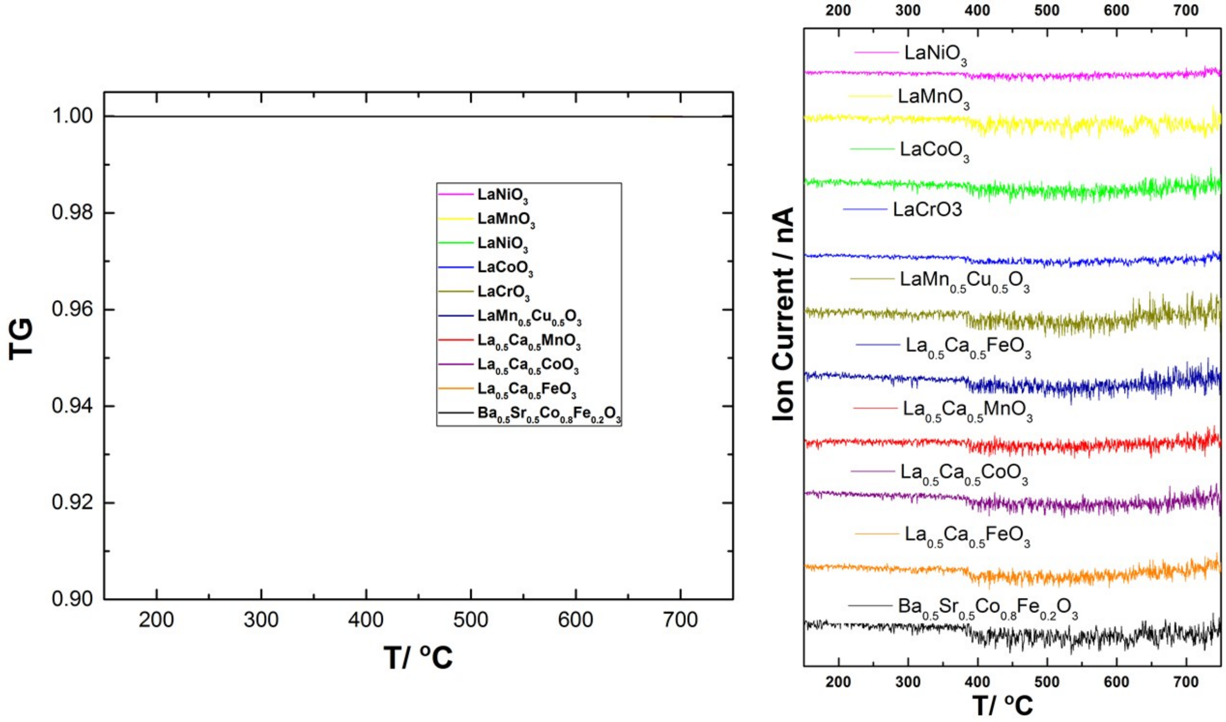

Figure S8. TGA-MS of as-synthesized perovskites with m/z=32 ion current displayed (All mass loss curves superimposed on top of one another)

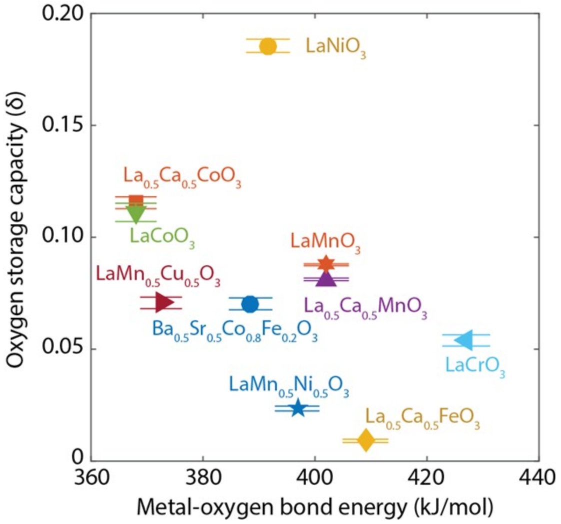

Figure S9. Plot of metal-oxygen (*B*—O) bond strength vs. oxygen storage capacity of each sample.

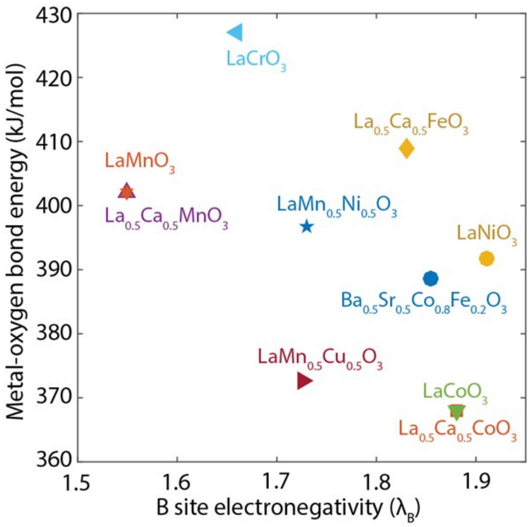

Figure S10. Plot of B site electronegativity vs. metal-oxygen (*B*—O) bond strength.

---

[1] G. Q. Jian, L. Liu and M. R. Zachariah, *Advanced Functional Materials*, 2013, **23**, 1341-1346.

[2] L. Liu and M. R. Zachariah, *Energy Fuels* 2013, **27**, 4977-4983.